Heliyon 10 (2024) e37472

Contents lists available at ScienceDirect

Heliyon

journal homepage: www.cell.com/heliyon

Research article

Dose prediction for cervical cancer in radiotherapy based on the beam channel generative adversarial network

Hui Xie [a,b], Tao Tan [b], Hua Zhang [c], Qing Li [a,d,e,*]

[a] Department of Radiation Oncology, Affiliated Hospital (Clinical College) of Xiangnan University, Chenzhou, 423000, PR China
[b] Faulty of Applied Sciences, Macao Polytechnic University, Macao, 999078, PR China
[c] Beijing Linking Med Technology Co., Ltd., No.9, Fenghaodong 2C-5, Haidian, Beijing 100089, PR China
[d] Key Experimental Project of Higher Education Institutes in Hunan Province(Key Laboratory of Tumor Precision Medicine), Chenzhou, 423000, PR China
[e] College of Medical Imaging, Laboratory Diagnostics, and Rehabilitation, Xiangnan University, Chenzhou, 423000, PR China

ARTICLE INFO

Keywords:
Deep learning
Beam-channel generative adversarial network (Bc-GAN)
Dose prediction
Cervical cancer (CC)
Radiotherapy

ABSTRACT

Background: Existing deep learning methods, such as generative adversarial network (GAN) technology, face challenges when dealing with mixed datasets, which involve a combination of Intensity Modulated Radiotherapy (IMRT) and Volumetric Modulated Arc Therapy (VMAT). This issue significantly complicates the application of dose prediction in the field of radiotherapy. In this study, we propose a novel approach called beam channel GAN (Bc-GAN) to address the task of radiation dose prediction for mixed datasets. Bc-GAN introduces a dose prediction calculation method that requires less precision. By defining an approximate range for dose prediction, Bc-GAN limits the physical range of GAN prediction, resulting in more reasonable dose distribution predictions.

Methods: We adopt a beam angle weighting method to determine the beam angle in the dose calculation. The dose of the beam with the highest weight is calculated using medical images and is then inputted into the artificial intelligence dose prediction model as the input channel. Additionally, we collect data from a total of 346 patients with Cervical Cancer (CC) for dataset. After cleaning the data, we exclude 51 cases with incomplete organ delineation, leaving us with 295 cases (IMRT: VMAT = 137:158) randomly divided into three sets: the training set, the validation set, and the test set, with proportions of 205:60:30, respectively. The assessment of model predictions was conducted via an analysis of dose distributions on the tomographic plane, dose volume histogram (DVH), and dosimetric parameters within the target zones and organs at risk (OAR).

Results: After DVH analysis, minimal discrepancy was found between predicted and actual dose distributions in PTV and OAR. The predicted distribution aligned with clinical standards. Dosimetric parameters for PTV were generally lower in the predicted model, except for homogeneity index (HI) (0.238 ± 0.024, P = 0.017) and Dmax (53.599 ± 0.710 Gy, P = 1.8e-05). The prediction model varied in estimating doses for six organs. Specifically, small intestine showed higher V_{20} (67.92 ± 51.64 %, P = 0.019) and V_{30} (57.171 ± 1.213 %, P = 0.024) than manual planning. A similar trend was seen in colon's V_{30} (37.13 ± 61.14 %, P = 0.016). However,

* Corresponding author. College of Medical Imaging, Laboratory Diagnostics, and Rehabilitation, Xiangnan University, Chenzhou, 423000, E-, PR China.
E-mail address: xnxyliqing@163.com (Q. Li).

https://doi.org/10.1016/j.heliyon.2024.e37472
Received 18 March 2024; Received in revised form 3 September 2024; Accepted 4 September 2024
Available online 7 September 2024

predicted bladder V30 (87.51 ± 41.44 %, P = 2.03e-16) was lower, indicating significant dosimetric differences.

Conclusion: Overall, this study presents an innovative prediction method for CC in radiotherapy using the Bc-GAN model, addressing the challenges posed by different radiotherapy techniques. The proposed approach allows IMRT and VMAT in radiotherapy to be used as training sets, enabling the potential for large-scale engineering and commercialization applications of artificial intelligence (AI). The Bc-GAN-based prediction method for CC in radiotherapy not only reduces the amount of data needed for the training set but also expedites the model generation process. This approach can be applied to guide the development of clinical radiation therapy plans. Furthermore, future studies should consider extending the dose prediction method to encompass other types of tumors.

1. Introduction

Cervical cancer (CC) is a prevalent disease worldwide [1], and it remains the leading cause of cancer-related deaths among women in developing nations [2]. The treatment options for cervical cancer are highly individualized, especially when dealing with locally advanced cervical cancer (LACC), i.e., stages IB2, IIA, and IIB. The choice of treatment methods is particularly crucial. On one hand, external beam radiation therapy and brachytherapy combined with cisplatin-based chemotherapy (CRT) have been proven beneficial for patients. On the other hand, there is ongoing discussion in the medical community about the potential for neoadjuvant chemotherapy combined with surgery (NACT + S) to provide greater benefits to patients in terms of disease-free survival (DFS) [3]. Some studies have further indicated that for patients with cervical cancer stages IB2 to III, radical hysterectomy following NACT is considered an effective alternative to concurrent CRT. This provides new options for clinical treatment, making treatment plans more diverse [4]. However, regardless of the controversies and discussions, chemotherapy, radiotherapy, and surgery remain the core treatment modalities for CC. These fundamental treatment methods play an indispensable role in the comprehensive treatment of CC, providing patients with powerful weapons to fight the disease. Radiotherapy plays a crucial role in the treatment of CC, with approximately 80 % of patients in various clinical stages undergoing this treatment modality [5,6]. In external beam radiation therapy, the goal is to deliver a higher dose of radiation to the tumor site by generating multiple radiation beams from various angles that converge precisely at the tumor. Currently, two commonly employed techniques in external beam radiation therapy for CC are intensity-modulated radiation therapy (IMRT) and volumetric modulated radiation therapy (VMRT) [7].

Appropriate dose constraints must be established for both the target area and the organs at risk (OAR), regardless of whether IMRT or VMRT is utilized. The determination of constraint conditions is tantamount to establishing the required objective function during the design phase of the IMRT or VMRT plan [8]. Once the dose constraint conditions are determined, an optimized IMRT or VMRT plan can be derived through iterative optimization of the objective function. The dose constraints for the target area and OAR can be derived from the dose distribution map. Therefore, this study aims to focus on developing a dose distribution prediction model based on deep learning.

In the sphere of radiation therapy, the application of dose distribution prediction has been extensive. In 2021, reports were published regarding the assessment of the influence of patients' respiration on radiotherapy through the utilization of dose prediction models [9]. Osman et al. devised an attention-gated 3D U-Net dose prediction model to facilitate radiotherapy planning [10]. Currently, dose prediction models can be broadly categorized into two types: neural network models based on backpropagation (BP) and deep neural network models [9,10]. The BP neural network model seeks to find the relationship between the dose of each voxel in the region of interest (ROI) and the geometric anatomical characteristics of the patient through training. However, this method may lead to incorrect estimation of the input dose to the BP neural network, affecting the dose output of the corresponding voxel [11]. In order to tackle this matter, researchers have suggested utilizing 3D deep neural networks, such as U-net [10], DenseNet [12], and HD U-net [13], for dose prediction. Recently, a scholar has proposed leveraging the Pix2pix model of Generative Adversarial Networks (GAN) to forecast dosages, which has proven to be successful [14]. Pix2pix is GAN-based image translation model, which facilitates the allocation of three-dimensional (3D) dose based on the patient's geometric anatomy and organ prediction model [15]. According to previous studies, GAN models have demonstrated the capability to accurately predict the distribution of radiotherapy doses for pharyngeal cancer [16,17]. In line with this, Fan J., a group of Chinese researchers, utilized this model to forecast the dose distribution for patients undergoing IMRT, yielding significant outcomes [18]. Scholars have proposed the Multi-class Generative Adversarial Network (Mc-GAN) framework, which is an end-to-end GAN framework that integrates multiple constraints, aiming to improve the accuracy of automated dose prediction [19]. This framework has exhibited promising results in a dataset containing 42 patients CC and 130 patients with rectal cancer.

Previous GAN models were limited to datasets of a single radiotherapy technique, rendering them compatible with either IMRT or VMRT exclusively. Furthermore, these models were incapable of accommodating different beam angles within the same technique, necessitating separate datasets for each beam angle. Consequently, these challenges underscore the necessity for larger datasets to effectively train the GAN model. The clinical application of GAN models is hindered by the challenge of collecting radiotherapy data of the same technology type in the clinical setting. To overcome this challenge, this study introduces a novel approach, namely the Beam Channel Generative Adversarial Networks (Bc-GAN), for predicting the radiation dose distribution in CC. The dataset used in our study consists of a combination of IMRT and VMAT techniques. This particular dataset offers several benefits, including the substantial reduction in required training data and the ability to overcome the limitations imposed by using a single type of radiotherapy

technique. Consequently, the application scope of our model is expanded.

2. Materials and methods

2.1. Definition of beam channel

To tackle the challenges in handling mixed datasets in existing GAN, we have proposed the concept of a beam channel. The beam channel is a technique that calculates the dose of beams with higher weights using the patient's medical images and subsequently transforms the outcomes into inputs for the artificial intelligence dose prediction model.

The method for generating a beam path is described as follows. Initially, the three-dimensional planning target volume (3D-PTV) and the beam angle data of the radiation therapy patient are acquired. Subsequently, the beam angles are projected onto the PTV, where a value of 1 is assigned to the scenes within the channel region, while the remaining scenes are assigned a value of 0. Finally, we selected typical IMRT and VMRT plan as the dataset, and the parameters of the IMRT plan were used as the beam channel parameters. In this study, the methods for dose calculation included: pencil beam convolution (PBC), folded convolution, and Monte Carlo (MC) [20]. Based on the aforementioned discussion, it can be concluded that the PBC algorithm, despite being the simplest and least accurate, sufficed for the dose calculation. Among the three algorithms mentioned, PBC is the simplest one, assuming that the radiation is composed of finite beams, which are known as 'finite pencil beams'. The dose distribution on any given spatial grid point was generated by the combined contribution of direct illumination and scattering from all pencil beams. The PBC algorithm was expressed by the following mathematical model (Equation (1)) [21].

$$D(x,y,z)=\iint_{F}\Psi(x',y')\frac{K_w(x-x',y-y')}{\rho}dx'dy' \quad (1)$$

ρ represented the density; Ψ meant the probability density function distribution of the radiation source, i.e., the energy fluence; K_w meant the pencil beam, and the homogeneous water phantom was calculated in advance by other means (measurements, Monte Carlo simulations, analytical calculations, etc)

2.2. Bc-GAN model

The GAN model was originally conceived by Goodfellow [22] and is comprised of a generator (G) and a discriminator (D) network. The G is tasked with producing images, while the D is responsible for distinguishing between real and generated images (with real images labeled as 1 and generated images as 0). Through a competitive process, both the G and D improve their abilities. Specifically, the realism of the generated images by G increases, while D becomes more proficient at identifying real α images. In this study, our objective was to develop a min-max model that reduces D's judgment ability on G while maximizing D's own ability.

This study introduces the concept of Bc-GAN for predicting radiation doses in mixed datasets. As illustrated in Fig. 1 (A), Bc-GAN takes an image as input and generates a synthetic image. This generated image accurately captures the desired conditions and facilitates the transformation between images.

In the Bc-GAN model (Fig. 1 (A)), four channels are generated when the input condition Y is provided (consists of a patient's CT slices, pelvic organ annotation information, dose information, and radiation beam angle information). These channels consist of three for dose images (consists of a patient's CT slices, pelvic organ annotation information, dose information) and one for beams. The U-net network of the G is utilized to acquire predictions of the dose images, namely fake_x and fake_y. The fake_x images, produced by the G, seamlessly integrate the patient's CT slices, comprehensive annotation details for pelvic organs, dose information, and crucial angle information of the radiation beam. And, fake_y represents the simulated dose information calculated based on the beam angle information, utilizing the PBC model (as illustrated in Fig. 1 (B)). Real_x represents the actual dose information.

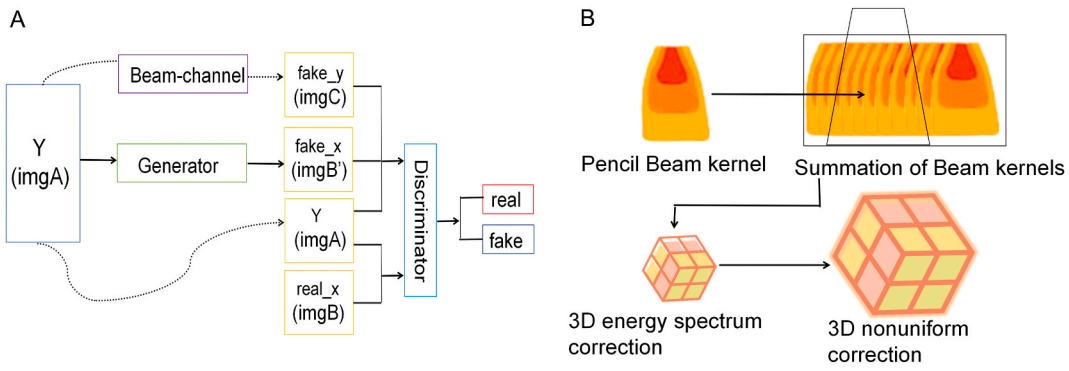

Fig. 1. The Beam Channel Generative Adversarial Networks.
A: Beam Channel Generative Adversarial Networks; B: Beam channel using PBC model.

In the Bc-GAN model, the G function utilizes only the input Y (imgA) as a condition. Y undergoes decoding by G, employing the U-net structure (Fig. 2), in order to generate the synthesized image fake_x (imgB'). For discriminator (D) (Fig. 3), in addition to the conditional information Y, the input also encompasses imgB' or the real image real_x (imgB). Moreover, in the PBC model, the beam channel-integrated condition Y results in the generation of fake_y (imgC) as depicted in equation (1). The generation of imgC is based on a physical model, thereby effectively constraining the image within the physical range. As a result, the input for the D comprises fake_y' (the simulated dose distribution), fake_x (the generated images incorporating various information), Y, and real_x' (the actual dose information). This constraint proves advantageous for image-to-image transformations.

In the Bc-GAN model (Fig. 1(A)), four channels are generated when the input condition Y is provided. These channels consist of three for dose images and one for beams. By traversing the U-Net of G alongside the beam channel, the model can generate predictions of dose images (fake_x and fake_y).

The actual doses (Y and real_x) and the generated predicted doses (fake_x and fake_y) were supplied as input to D to distinguish between their disparities and produce the outcome. The structures of G and D utilized in this study were delineated in detail as follows.

The beam channel served as the dose calculation engine of the PBC model, as illustrated in Fig. 1 (B). The calculation methods consisted of four steps.

1. MC Algorithm for Beam Acquisition: The first step involved using a Monte Carlo algorithm to acquire the finite pencil beams in a water phantom. Monte Carlo simulations are renowned for their accuracy in modeling complex physical processes, including the interactions of radiation with matter. In this case, the simulations provided detailed information about the dose deposition patterns of individual pencil beams in a water environment.
2. 3D Dose Map Generation: The next step was to generate a 3D dose map by summing up the beam kernels and incorporating imgA, which contained the 3D CT (Computed Tomography) scan of the patient along with the contours of organs and targets. This step utilized the discrete forms of Equation (1) to overlay the dose patterns from individual pencil beams onto the patient's anatomical structure. The result was a 3D dose distribution map tailored specifically to the patient's anatomy.
3. Adjustment for 6 MV Photon Energy Spectrum: In radiation therapy using 6 MV photons, the exact energy spectrum is not always required for dose calculations. However, to ensure accuracy, the calculations from the previous step could be adjusted using the corresponding 6 MV photon energy spectrum of Elekta Synergy (Elekta Oncology Systems, Crawley, UK). This adjustment accounted for the slight differences in energy deposition patterns between different photon energies, ensuring that the dose predictions matched the actual therapeutic beam.
4. Non-Uniformity Correction for Human Body: The final step involved correcting for the non-uniformity of the human body in 3D. This correction was based on the relationship between CT density and the dose deposition pattern. Since human tissue has varying densities, the same dose from a pencil beam may deposit differently in different tissues. By considering the CT density information, the PBC model was able to perform non-uniformity corrections to more accurately predict the dose distribution within the patient's body. Notably, this correction did not require knowing the specific CT density values for each tissue type, but relied on the relative differences in density to adjust the dose calculations.

2.3. Bc-GAN dose prediction model for cervical cancer

An 8-level U-net was utilized to map images to our sampled data in processing the CC dataset (Fig. 2). The network architecture comprises two parts: feature extraction and upsampling. The input consists of four-channel, 256 x 256 pixel images. In the feature extraction part, a 3 x 3 convolution is applied at each level, succeeded by a 2 x 2 maximum pooling to reduce the dimensions of the 256 x 256 pixel features to 1 x 1 pixels. In the upsampling part, the curved structure used at each level is transformed back to the original data, and upon transitioning to the next level, the maximum pooling layer is substituted with a 2 x 2 upsampling layer to restore the image to its original size. The approach illustrated in Fig. 4 aims to preserve fundamental features and prevent loss of image details.

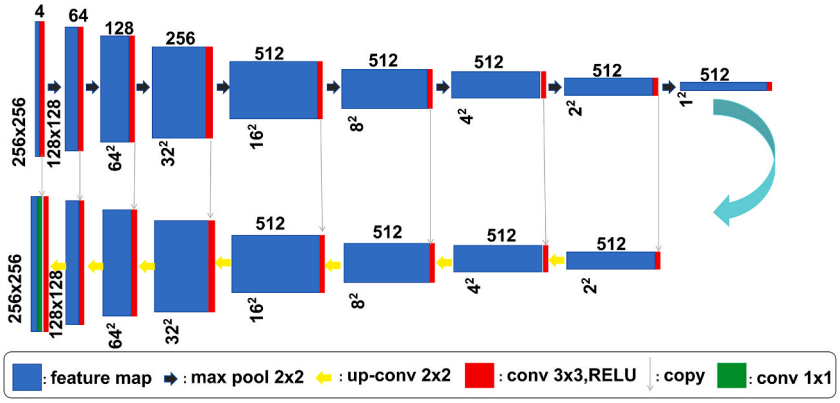

Fig. 2. Generator model using 8-layer 2D U-net.

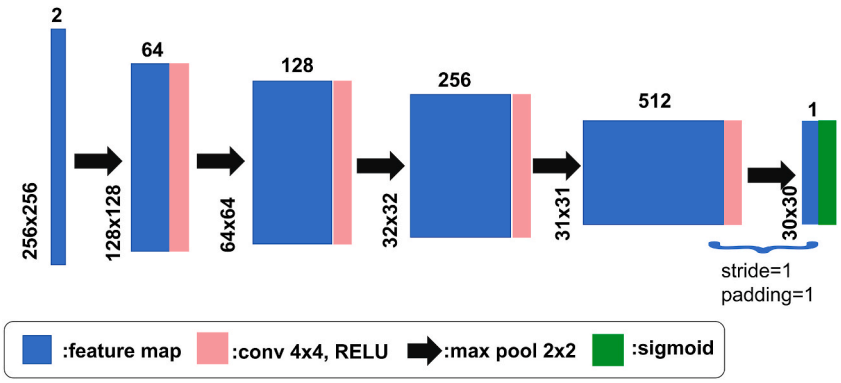

Fig. 3. Discriminator identification process (a Markov process).

The final output image is a 256 x 256 x 1 dose map.

The Adam optimization algorithm [23] is employed as the optimizer to minimize the loss function during the training phase. The learning rate is set to 2×10^{-3}, and the training process iterates for 1000 times.

The PatchGAN (D) in Fig. 3 was employed to assess the quality of image generation. The PatchGAN operates under the premise that individual patches within an image are independent, and thus it discriminates between real and fake patches of size N x N using D. Following the Pix2pix approach of dividing the image into N x N patches, each patch is evaluated by D. Finally, the output is the average of the evaluations of all patches in the image. Considering an input of 256x256, the optimal judgment outcome was achieved with a patch size of 70x70.

2.4. Datasets and data preprocessing

Our study included a total of 346 patients with CC for analysis. After performing data cleaning, 51 patients with organ dysfunction were excluded, leaving 295 cases (137 treated with IMRT and 158 treated with VMAT) for constructing the model. These patients were randomly divided into a training set, a validation set, and a test set in a ratio of 7:2:1 (205 patients in the training set, 60 in the

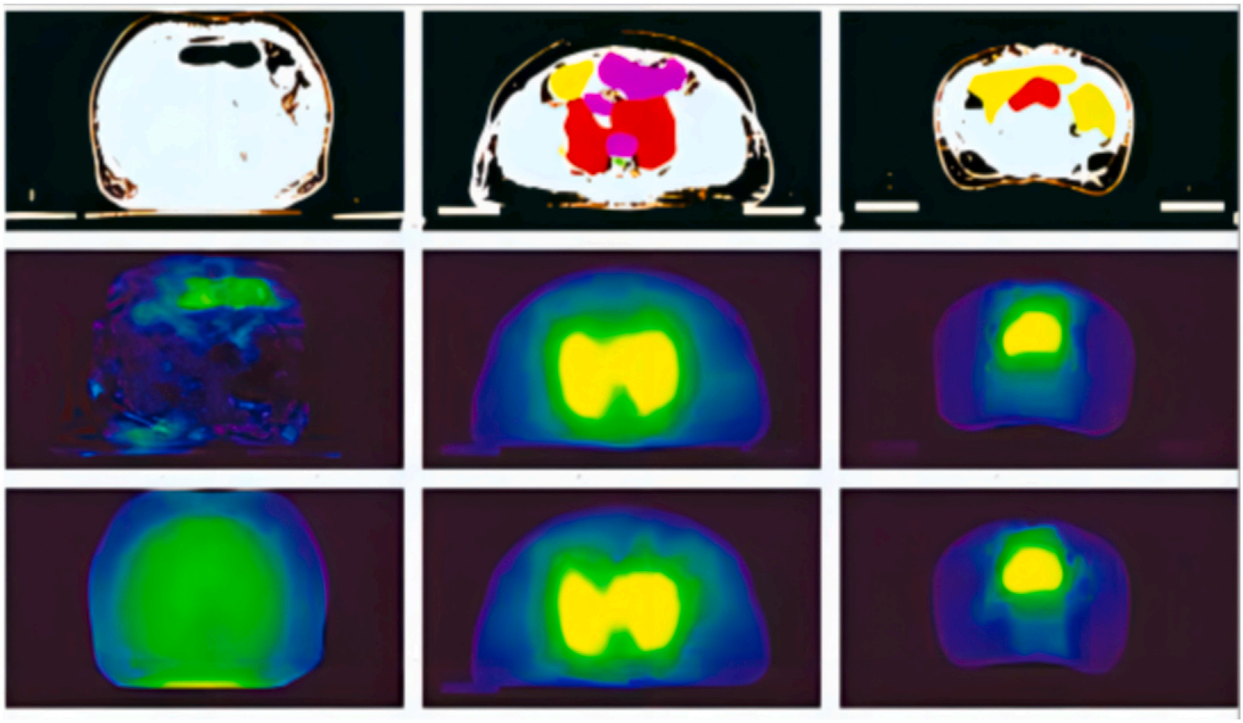

Fig. 4. Comparison examples of predicted and true dose; the plot was obtained by random sampling; the first line: CT images; the second line: the true dose map; the third line: the predicted dose map.

validation set, and 30 in the test set). The mixed dataset was exported in Digital Imaging and Communications in Medicine (DICOM) format by MONACO treatment planning system (Elekta, Crawley, UK). However, due to medical information security reasons, these mixed datasets cannot be made publicly available. All patient data in this study underwent complete de-identification, and all procedures were conducted in accordance with the relevant standards and regulations established by the respective organization. The computer system used for the analysis was Ubuntu 20.04, equipped with an Intel® Core™ i3-8350K CPU running at 4.00 GHz, a GTX1080Ti graphics card, Python 3.6 as the integrated development environment (IDE), and TensorFlow 1.0 [24] as the platform.

The data preprocessing phase encountered a significant challenge related to inconsistent naming conventions between different radiotherapy physicists. As a result, the computer was unable to accurately identify the ROI for organs and PTV. To address this issue, we implemented a standardization process for ROI names and aliases, alongside the establishment of a uniform naming dictionary for information extraction. Additionally, each 3D CT image underwent segmentation into 256 × 256 pixel 2D slices. The generator then utilized these individual CT image slices to predict the dose distribution along the same plane, without considering the vertical relationship between slices. This process was repeated for each slice until a complete 3D dose distribution was obtained. For our experiment, the training and validation sets consisted of all 2D slices from 3D CT images of 205 and 60 patients, respectively. The remaining 30 patients' CT images were utilized as test data for dose prediction. Fig. 4 provides a visual representation of this process.

2.5. Evaluation method

The evaluation of the results of dose prediction is based on the comparison of various parameters, including the dose distribution and dose volume histogram (DVH) of each section. (1) Target dose parameters: D_1 (the maximum dose received by 1 % volume of the PTV), D_2, D_{98} (the minimum dose received by 98 % volume of the PTV), D_{95}, Mean dose (Dmean) and Maximum dose (Dmax). (2) The conformity index (CI) is used to evaluate the conformality of the isodose line with the target PTV. The CI range is 0–1, and the larger the CI, the better the conformality of the target area. The calculation formula is shown in Equation 2. (3) The homogeneity index (HI) of the target area reflects the uniformity of the dose distribution within the target area. The HI range is 0∼1, and the smaller the value, the more uniform the dose within the target area. The calculation formula for HI is shown in Equation (3). In this study, we compared the predicted dose distribution for critical organs with the planned dose distribution map for these organs, including small intestine, colon, rectum, bladder, and both femoral heads. Dmax and Dmean doses as well as volumes irradiated with doses of 5, 10, 20, 30, and 40 Gy (V_5, V_{10}, V_{20}, V_{30}, V_{40}) were identified for each organ.

$$CI = \left(\frac{TV_{RI}}{TV}\right) \times \left(\frac{TV_{RI}}{V_{RI}}\right) \tag{2}$$

TV_{RI}: The target volume enclosed by the prescription dosage line; TV:target volume; V_{RI}:The volume of prescription dosage packaging

$$HI = \frac{(D_2 - D_{98})}{D_{50}} \tag{3}$$

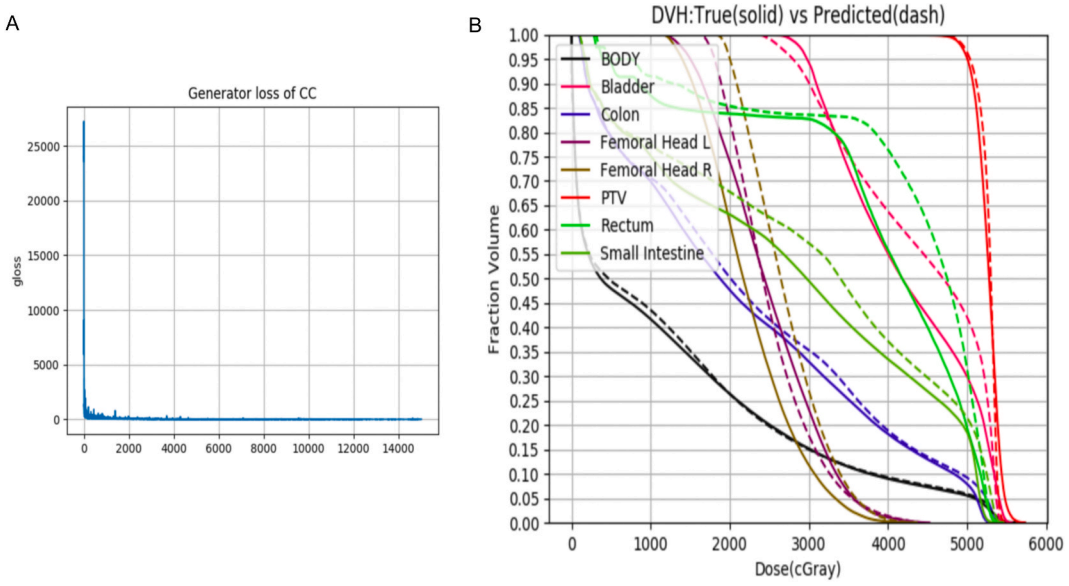

Fig. 5. A: loss curve during training; B: Comparison of the predicted DVH and the true DVH of one case.

2.6. Statistical analysis

We conducted statistical analysis using Python, where we applied the Shapiro-Wilk test to examine the normality of the data sets, followed by paired t-tests for data sets that meet the normal distribution condition, and Wilcoxon signed-rank tests for data sets that do not meet the normal distribution condition. A statistically significant difference is considered when the p-value is less than 0.05.

3. Results

3.1. Model training

A total of 205 training samples (IMRT: VMRT = 105:100), comprising 40 epochs (cycles on cases) were utilized in this study. The training process took approximately 179 h. Notably, this study's model achieved good results without the need for further adjustment of the sample parameters. Fig. 5(A) presents the loss plot of the generated model. Initially, the loss of the training model exhibited a significant decrease, but after reaching 700 iterations, the decrease became gradual. The curve smoothly converged after 40 epochs, with minimal fluctuation in the loss curve during continued training.

3.2. Dose volume histogram comparison

There are 30 patients in the test data set (IMRT: VMRT = 11:19). The comparison results of the predicted dose volume histogram (DVH) and the actual DVH are presented in Fig. 5(B). By human observation of the DVH, there was little difference between the predicted and actual dose distributions on the PTV and OAR. The predicted dose distribution is in full compliance with the clinical requirements.

3.3. Comparison of dosimetric parameters for PTV

The dosimetric parameters of the predicted dose distribution map once again demonstrate the accuracy of our newly proposed model. Numerically, the dosimetric parameters for the PTV in the predicted model are generally lower than those in the manually created dose distribution. However, there are no significant statistical differences, except for the HI (0.238 ± 0.024, P = 0.017) and Dmax (53.599 ± 0.710 Gy, P = 1.8e-05). These findings indicate that the dose prediction model effectively controls the hotspots of the PTV and results in a more uniform dose distribution, as presented in Table 1.

3.4. Comparison of dosimetric parameters for OAR

The prediction model yielded varying results regarding the doses predicted for six organs at risk. Specifically, the V_{20} (67.92 ± 51.64 %, P = 0.019) and V_{30} (57.171 ± 1.213 %, P = 0.024) doses for the small intestine were higher than those established through manual planning. A similar trend was observed for the colon, with V_{30} (37.13 ± 61.14 %, P = 0.016). However, the predicted doses for the bladder V_{30} (87.51 ± 41.44 %, P = 2.03e-16) were lower than the manually planned doses, indicating evident dosimetric disparities. Consequently, the prediction model exhibits superior efficacy in controlling high-dose levels when compared to manually developed dose distributions, yet proves less effective in controlling low-dose levels, as demonstrated in Table 2.

4. Discussion

This study aimed to investigate the feasibility of utilizing deep learning methods with a mixed training dataset (IMRT and VMRT) to generate accurate predictions of radiotherapy dose in high quality. The distribution of dose plays a crucial role in determining the efficacy of radiotherapy treatment [25]. Physicists spend substantial time and effort on dose optimization during the radiation therapy planning process. Literature suggests that an optimal dose distribution chart assists physicists in efficiently designing planning parameters, thus enhancing work efficiency [26]. Our newly proposed Bc-GAN model demonstrates skills comparable to, and in some cases even surpassing, those of physicists with 10 years of experience in dose distribution prediction. Crucially, the model exhibits superior performance in regulating hotspots within the PTV and reducing high doses to OAR (Tables 1 and 2). As a result, this research breakthrough can effectively guide physicists in optimizing radiotherapy dosage, thereby not only significantly reducing manpower costs but also enhancing the level of radiation dose distribution, thereby holding significant clinical value.

Table 1
Comparison of manual and predicted does of PTV ($\bar{x} \pm SD$).

	Dmax (Gy)	Dmean (Gy)	D1 (Gy)	D2 (Gy)	D95 (Gy)	D98 (Gy)	CI	HI
Manually	54.403 ± 0.722	51.629 ± 0.741	51.503 ± 0.864	51.713 ± 0.802	49.126 ± 0.584	47.995 ± 0.652	0.744 ± 0.066	0.261 ± 0.038
Prediction	53.599 ± 0.710	52.568 ± 0.919	52.483 ± 0.878	52.469 ± 0.924	48.89 ± 0.637	47.837 ± 0.583	0.768 ± 0.051	0.238 ± 0.024
p	1.8e-05	0.100	0.300	0.059	0.1229	0.2996	0.130	0.017

Table 2
Comparison of manual and predicted does of OAR ($\bar{x} \pm SD$).

OAR		Dmax (Gy)	Dmean (Gy)	V5 (%)	V10 (%)	V20 (%)	V30 (%)	V40 (%)
Small Intestine	Manually	53.108 ± 0.665	24.487 ± 0.930	93.619 ± 1.468	78.177 ± 1.211	57.818 ± 1.518	53.254 ± 1.626	38.06 ± 1.644
	Prediction	51.771 ± 0.826	25.579 ± 0.859	94.959 ± 1.8	78.266 ± 1.518	67.925 ± 1.642	57.171 ± 1.213	39.928 ± 1.789
	P	0.351	0.511	0.104	0.147	0.019	0.024	0.114
Rectum	Manually	53.067 ± 0.740	38.700 ± 2.088	99.158 ± 1.049	87.061 ± 1.664	78.171 ± 1.833	83.564 ± 1.700	56.815 ± 0.948
	Prediction	51.800 ± 0.805	40.871 ± 1.834	99.453 ± 0.255	92.236 ± 2.102	79.724 ± 1.975	83.090 ± 1.630	61.857 ± 1.789
	P	0.065	0.711	0.140	0.745	0.103	0.276	0.134
Colon	Manually	50.952 ± 0.720	24.218 ± 0.980	87.526 ± 1.924	79.068 ± 0.864	47.866 ± 1.961	32.597 ± 2.047	23.273 ± 1.794
	Prediction	49.954 ± 0.889	25.562 ± 0.821	87.937 ± 1.897	79.035 ± 1.175	48.934 ± 2.154	37.136 ± 1.142	23.197 ± 1.864
	P	0.926	0.171	0.382	0.866	0.059	0.016	0.899
Bladder	Manually	53.077 ± 0.657	33.742 ± 1.235	100	100	100	93.14 ± 1.942	57.64 ± 1.738
	Prediction	51.767 ± 0.754	34.543 ± 0.892	100	100	100	87.508 ± 1.437	58.206 ± 1.826
	P	0.948	0.069				2.03e-16	0.273
Left Femoral Head	Manually	43.28 ± 0.648	24.147 ± 0.718			75.075 ± 1.160	18.168 ± 1.383	2.998 ± 1.734
	Prediction	43.080 ± 0.615	22.649 ± 2.458			78.983 ± 1.968	23.093 ± 1.342	2.942 ± 1.766
	P	0.276	0.113			0.102	0.084	0.843
Right Femoral Heads	Manually	33.11 ± 0.509	14.34 ± 0.882			64.162 ± 2.814	12.959 ± 1.576	3.019 ± 2.051
	Prediction	32.947 ± 0.607	15.768 ± 0.932			66.764 ± 1.733	15.165 ± 1.708	3.396 ± 1.426
	P	0.206	0.497			0.081	0.073	0.114

In recent years, the implementation of deep learning techniques in the field of radiation dose prediction has significantly improved the accuracy of dose estimation, reaching a level that is applicable in clinical settings. For instance, Bohara et al. utilized deep learning methods to forecast the clinical dose distribution of patients undergoing IMRT for prostate cancer, and their results closely mirrored the gold standard [27]. Similarly, Song et al. employed the DeepLav3+ network to predict the dose distribution in VMAT plans for rectal cancer, achieving predicted results that align with clinical requirements [28]. Their study yielded a mean square difference of 0.001 and a normalized dose difference of 0.4 %. In addition to improved accuracy, the utilization of dose prediction outcomes has the potential to streamline the physical design planning process, potentially saving an average of 15 min for junior physicists [28]. Ravari ME and his team used a deep learning model to predict the radiation dose distribution in left breast cancer patients, and the predicted results were almost identical to the actual doses [29].

There has been extensive research conducted on the prediction of radiation therapy dosage for CC. Yu et al. employed a 3D deep residual neural network and 3DUnet to successfully predict the distribution of radiation therapy dosage in postoperative CC patients undergoing VMRT [30]. Chen et al. conducted a study involving 140 CC patients who underwent IMRT, and they predicted the radiation therapy dosage using a CNN deep learning model. Among the 20 patients in the test set, the dosage distribution met the clinical requirements in 14 cases (70 %) [31]. Zhang et al. developed a 3D-Unet dosage prediction model to predict the three-dimensional dosage distribution of VMAT for CC, and they also examined its performance in predicting dosage for endometrial cancer, which demonstrated a strong agreement between the predicted and actual dosage [32]. Tang et al. similarly utilized a deep learning dosage prediction model based on 3D-Unet to accurately forecast the dosage distribution of VMAT for CC, and it proved to be equally effective for cases of endometrial cancer [33]. In our study, we conducted a bold innovation by proposing a novel Bc-GAN model and attempting to use a hybrid dataset (IMRT and VMRT data) for dose prediction. This approach not only reduces data collection issues but also minimizes training costs. It is also in line with the current trend of developing "big models". Therefore, our research is more innovative.

Existing research has shown that incorporating beam information features is effective in improving the accuracy of dose prediction. A study by Barragán-Montero AM found that when beam channel information is included in the prediction model, the model's prediction accuracy for dose distribution is higher than models without beam channel information [34]. A 3D deep learning model developed by Zhou and others was used to predict the radiation dose distribution in 122 postoperative rectal cancer patients undergoing IMRT treatment, and beam channel information was incorporated into the model's input [35]. The model achieved an average prediction deviation range of −1.94 %–1.58 %, with an overall mean absolute error (MAE) of 3.92 ± 4.16 %. No statistically significant differences were observed in any of the indicators, and the model outperformed models without beam channel information.

In our study, we observed a significant improvement in predictive accuracy with the incorporation of Beam channel information. We assessed the performance of the Bc-GAN model in dose prediction by comparing the dosimetric parameters of predicted and actual doses in the test set. Notably, the comparison of DVH graphs revealed minimal disparity between the predicted and actual doses derived from manual planning. Further comparison of dosimetric parameters in the PTV and OAR demonstrated a high level of

consistency between our dose prediction model and the actual dose. Intriguingly, our predictive model exhibited excellent performance in managing hotspots in the PTV and high doses in OAR, suggesting that optimization in radiotherapy treatment planning could result in a more desirable radiation dose distribution. This can be attributed to our novel utilization of a hybrid dataset, which combined the advantages of both VMRT and IMRT techniques. VMRT technique excels in terms of target coverage and uniformity [36], which explains the superior performance of our predictive model in the target area's HI (0.238 ± 0.024, $P = 0.017$) and Dmax (53.599 ± 0.710 Gy, $p = 1.8e\text{-}05$). However, we did identify slight discrepancies in several dosimetric parameters of six organs at risk compared to the actual doses from manual planning. These included V_{20} (67.92 ± 51.64 %, $P = 0.019$) and V_{30} (57.171 ± 1.213 %, $P = 0.024$) of the small intestine, V_{30} (37.13 ± 61.14 %, $p = 0.016$) of the colon. Despite these statistical differences, all values remain within the standards of radiation therapy and are clinically acceptable [37]. External radiation therapy involves the passage of radiation through the body surface to reach the target area, which necessitates a trade-off between the target area and organs at risk. If the dose distribution in the target area is favorable, the OAR may be compromised, and vice versa. This clarifies why our predictive model excelled in the dose distribution of the target area, resulting in a slightly less optimal dose distribution in OAR. It is worth noting that our model may have inherent limitations, leaving room for improvement in our dose prediction model. It is noteworthy that, due to hardware constraints during the experiment, we did not perform extensive parameter fine-tuning. As a result, there were slight deviations in predicting the dosage for critical organs. Nevertheless, it is important to highlight that our model achieved good results without requiring further adjustments to the sample parameters. This outcome further substantiates the validity of our research. Nevertheless, despite these imperfections, the overall accuracy of our newly proposed predictive model and its clinical significance are promising.

In this study, we have developed a clinically feasible dose prediction model that could benefit patients in the future. However, there is still room for improvement. In the process of building and training this model, we encountered several significant limitations. Firstly, as the patient data used for training were all from the same medical institution, it may significantly impact the model's robustness and generalizability, limiting its performance when facing different medical environments and patient populations. Secondly, the relatively small amount of mixed data we used further restricts the model's ability to learn from diverse data and enhance its performance. Additionally, our research faces another limitation, which is that we have only conducted in-depth research on cervical cancer. This means that the model's training and optimization may lack consideration for other types of tumors, thus limiting its application potential for a wider range of tumor types.We are more acutely aware that due to hardware resource constraints, our model has not yet achieved perfect levels in optimizing critical organs. While we have achieved some initial results, there is still significant room for improvement. To address these challenges, we will strive to further improve and optimize the model. We will work to collect data from more medical institutions and a wider range of patient groups to enhance the model's robustness and generalizability. At the same time, we will also seek more hardware resource support to handle the training requirements of larger datasets and improve the model's performance in optimizing critical organs. Furthermore, we will consider extending the research scope of the model to other types of tumors to further enhance its broad applicability and effectiveness in practical applications. We firmly believe that through continuous efforts and improvements, our model will be able to provide more comprehensive and accurate decision support for the medical field.

5. Conclusion

In this study, we innovatively proposed a method for predicting radiotherapy doses based on the Bc-GAN model, which addresses the issue of datasets from different radiotherapy techniques. In the dose prediction study of CC in radiotherapy, IMRT and VMAT can be considered as mixed data input models, rather than being limited to a single radiotherapy technique. This study not only enables large-scale engineering and commercial application of artificial intelligence but also has the potential to accelerate model generation. Furthermore, further studies could extend this approach to predict doses for more tumors. In the future, the Bc-GAN model could be used to predict radiotherapy doses for patients with various solid tumors, such as cervical cancer, lung cancer, breast cancer, and others.

Ethics approval and consent to participate

The study protocol was evaluated and approved by the Ethics Committee of Xiangnan University (No. 2023YXU014).

Consent for publication

N/A.

Funding

Funding: This study was supported by.

1. Science and Technology Funding Project of Hunan Province, China (Grant number: 2021SK52205)
2. Scientific Research Fund of Hunan Provincial Education Department, China (Grant number: 21A0524)
3. Scientific Research Project of Hunan Provincial Health Commission, China (Grant number: 202202084081)
4. Hunan Natural Science Foundation, China (Grant number: 2023JJ50410)
5. Macao Polytechnic University, Macau (Grant number: RP/FCA-15/2022).
6. The Science and Technology Development Fund of Macau SAR, Macau (Grant number:0105/2022/A)

Availability of data and materials

Data from this study will be accessible upon request from the corresponding author with legitimate justification.

Conflict of interest statement and consent for publication

The authors have no ethical, legal and financial conflicts related to the article. All authors read and approved the manuscript to publish.

CRediT authorship contribution statement

Hui Xie: Writing – review & editing, Writing – original draft, Data curation. **Tao Tan:** Visualization, Methodology. **Hua Zhang:** Visualization, Validation, Formal analysis. **Qing Li:** Writing – review & editing.

Declaration of competing interest

The authors declare the following financial interests/personal relationships which may be considered as potential competing interests: NO reports a relationship with NO that includes: non-financial support. NO has patent NO pending to NO. NO If there are other authors, they declare that they have no known competing financial interests or personal relationships that could have appeared to influence the work reported in this paper.

Acknowledgements

Not applicable.

References

[1] J. Miller, A. Dakic, M. Spurgeon, F. Saenz, B. Kallakury, B. Zhao, J. Zhang, J. Zhu, Q. Ma, Y. Xu, P. Lambert, R. Schlegel, A.T. Riegel, X. Liu, AIB1 is a novel target of the high-risk HPV E6 protein and a biomarker of cervical cancer progression, J. Med. Virol. 94 (8) (2022 Aug) 3962–3977, https://doi.org/10.1002/jmv.27795. Epub 2022 Apr 27. PMID: 35437795; PMCID: PMC9199254.

[2] W.L. Cai, W.D. Huang, B. Li, T.R. Chen, Z.X. Li, C.L. Zhao, H.Y. Li, Y.M. Wu, W.J. Yan, J.R. Xiao, microRNA-124 inhibits bone metastasis of breast cancer by repressing Interleukin-11, Mol. Cancer 17 (1) (2018 Jan 17) 9, https://doi.org/10.1186/s12943-017-0746-0. Erratum in: Mol Cancer. 2020 Jun 27;19(1):111. PMID: 29343249; PMCID: PMC5773190.

[3] C. Marchetti, A. Fagotti, V. Tombolini, G. Scambia, F. De Felice, Survival and toxicity in neoadjuvant chemotherapy plus surgery versus definitive chemoradiotherapy for cervical cancer: a systematic review and meta-analysis, Cancer Treat Rev. 83 (2020 Feb) 101945, https://doi.org/10.1016/j.ctrv.2019.101945. Epub 2019 Nov 29. PMID: 31838220.

[4] C. Marchetti, F. De Felice, A. Di Pinto, A. Romito, A. Musella, I. Palaia, M. Monti, V. Tombolin, L. Muzii, P. Benedetti Panici, Survival nomograms after curative neoadjuvant chemotherapy and radical surgery for stage IB2-IIIB cervical cancer, Cancer Res Treat. 50 (3) (2018 Jul) 768–776, https://doi.org/10.4143/crt.2017.141. Epub 2017 Jul 19. PMID: 28724282; PMCID: PMC6056954.

[5] N. Okonogi, M. Fukahori, M. Wakatsuki, Y. Ohkubo, S. Kato, Y. Miyasaka, H. Tsuji, T. Nakano, T. Kamada, Dose constraints in the rectum and bladder following carbon-ion radiotherapy for uterus carcinoma: a retrospective pooled analysis, Radiat. Oncol. 13 (1) (2018 Jun 25) 119, https://doi.org/10.1186/s13014-018-1061-7. PMID: 29941040; PMCID: PMC6019512.

[6] A.M. Perrone, M. Tesei, M. Ferioli, F. De Terlizzi, A.N. Della Gatta, S. Boussedra, G. Dondi, A. Galuppi, A.G. Morganti, P. De Iaco, Results of a phase I-ii study on laser therapy for vaginal side effects after radiotherapy for cancer of uterine cervix or endometrium, Cancers 12 (6) (2020 Jun 21) 1639, https://doi.org/10.3390/cancers12061639. PMID: 32575821; PMCID: PMC7352893.

[7] T. Kodama, S. Kudo, S. Hatanaka, M. Hariu, M. Shimbo, T. Takahashi, Algorithm for an automatic treatment planning system using a single-arc VMAT for prostate cancer, J. Appl. Clin. Med. Phys. 22 (12) (2021 Dec) 27–36, https://doi.org/10.1002/acm2.13442. Epub 2021 Oct 8. PMID: 34623022; PMCID: PMC8664139.

[8] A.H. Klopp, A.R. Yeung, S. Deshmukh, K.M. Gil, L. Wenzel, S.N. Westin, K. Gifford, D.K. Gaffney, W. Small Jr., S. Thompson, D.E. Doncals, G.H.C. Cantuaria, B. P. Yaremko, A. Chang, V. Kundapur, D.S. Mohan, M.L. Haas, Y.B. Kim, C.L. Ferguson, S.L. Pugh, L.A. Kachnic, D.W. Bruner, Patient-reported toxicity during pelvic intensity-modulated radiation therapy: NRG oncology-RTOG 1203, J. Clin. Oncol. 36 (24) (2018 Aug 20) 2538–2544, https://doi.org/10.1200/JCO.2017.77.4273. Epub 2018 Jul 10. Erratum in: J Clin Oncol. 2019 Mar 20;37(9):761. Erratum in: J Clin Oncol. 2020 Apr 1;38(10):1118. PMID: 29989857; PMCID: PMC6097832.

[9] C. McIntosh, L. Conroy, M.C. Tjong, T. Craig, A. Bayley, C. Catton, M. Gospodarowicz, J. Helou, N. Isfahanian, V. Kong, T. Lam, S. Raman, P. Warde, P. Chung, A. Berlin, T.G. Purdie, Clinical integration of machine learning for curative-intent radiation treatment of patients with prostate cancer, Nat Med 27 (6) (2021 Jun) 999–1005, https://doi.org/10.1038/s41591-021-01359-w. Epub 2021 Jun 3. PMID: 34083812.

[10] A.F.I. Osman, N.M. Tamam, Attention-aware 3D U-Net convolutional neural network for knowledge-based planning 3D dose distribution prediction of head-and-neck cancer, J. Appl. Clin. Med. Phys. 23 (7) (2022 Jul) e13630, https://doi.org/10.1002/acm2.13630. Epub 2022 May 9. PMID: 35533234; PMCID: PMC9278691.

[11] Q. Li, H. Tao, J. Wang, Q. Zhou, J. Chen, W.Z. Qin, L. Dong, B. Fu, J.L. Hou, J. Chen, W.H. Zhang, Warfarin maintenance dose Prediction for Patients undergoing heart valve replacement- a hybrid model with genetic algorithm and Back-Propagation neural network, Sci. Rep. 8 (1) (2018 Jun 26) 9712, https://doi.org/10.1038/s41598-018-27772-9. PMID: 29946101; PMCID: PMC6018790.

[12] R. Kapoor, W 4th Sleeman, J. Palta, E. Weiss, 3D deep convolution neural network for radiation pneumonitis prediction following stereotactic body radiotherapy, J. Appl. Clin. Med. Phys. 24 (3) (2023 Mar) e13875, https://doi.org/10.1002/acm2.13875. Epub 2022 Dec 22. PMID: 36546583; PMCID: PMC10018674.

[13] K. Miki, M. Kusters, T. Nakashima, A. Saito, D. Kawahara, I. Nishibuchi, T. Kimura, Y. Murakami, Y. Nagata, Evaluation of optimization workflow using custom-made planning through predicted dose distribution for head and neck tumor treatment, Phys. Med. 80 (2020 Dec) 167–174, https://doi.org/10.1016/j.ejmp.2020.10.028. Epub 2020 Nov 11. PMID: 33189047.

[14] S. Tahri, A. Barateau, C. Cadin, H. Chourak, S. Ribault, F. Nozahic, O. Acosta, J.A. Dowling, P.B. Greer, A. Largent, C. Lafond, R. De Crevoisier, J.C. Nunes, A high-performance method of deep learning for prostate MR-only radiotherapy planning using an optimized Pix2Pix architecture, Phys. Med. 103 (2022 Nov) 108–118, https://doi.org/10.1016/j.ejmp.2022.10.003. Epub 2022 Oct 19. PMID: 36272328.

[15] G.M. Conte, A.D. Weston, D.C. Vogelsang, K.A. Philbrick, J.C. Cai, M. Barbera, F. Sanvito, D.H. Lachance, R.B. Jenkins, W.O. Tobin, J.E. Eckel-Passow, B. J. Erickson, Generative adversarial networks to synthesize missing T1 and FLAIR MRI sequences for use in a multisequence brain tumor segmentation model, Radiology 299 (2) (2021 May) 313–323, https://doi.org/10.1148/radiol.2021203786. Epub 2021 Mar 9. Erratum in: Radiology. 2021 Jul;300(1):E319. PMID: 33687284; PMCID: PMC8111364.
[16] M. Mirza, S. Osindero, Conditional generative adversarial nets, arXiv preprint arXiv:1411.1784 (2014).
[17] Rafifid Mahmood, Aaron Babier, Andrea McNiven, Adam Diamant, Timothy C.Y. Chan, Automated treatment planning in radiation therapy using generative adversarial networks, Proceedings of Machine Learning Research[J] 85 (2018) 1–14.
[18] J. Fan, J. Wang, Z. Chen, C. Hu, Z. Zhang, W. Hu, Automatic treatment planning based on three-dimensional dose distribution predicted from deep learning technique, Med. Phys. 46 (1) (2019 Jan) 370–381, https://doi.org/10.1002/mp.13271. Epub 2018 Nov 28. PMID: 30383300.
[19] B. Zhan, J. Xiao, C. Cao, X. Peng, C. Zu, J. Zhou, Y. Wang, Multi-constraint generative adversarial network for dose prediction in radiotherapy, Med. Image Anal. 77 (2022 Apr) 102339, https://doi.org/10.1016/j.media.2021.102339. Epub 2021 Dec 24. PMID: 34990905.
[20] T. Krieger, O.A. Sauer, Monte Carlo-versus-pencil-beam-/collapsed-cone-dose calculation in a heterogeneous multi-layer phantom, Phys. Med. Biol. 50 (5) (2005) 859.
[21] A. Ahnesjö, M.M. Aspradakis, Dose calculations for external photon beams in radiation therapy, Phys. Med. Biol. 44 (11) (1999) R99.
[22] I. Goodfellow, Nips 2016 tutorial: generative adversarial networks, arXiv preprint arXiv:1701.00160 (2016).
[23] I.K.M. Jais, A.R. Ismail, S.Q. Nisa, Adam optimization algorithm for wide and deep neural network, Knowledge Engineering and Data Science 2 (1) (2019) 41–46.
[24] Martín Abadi, Paul Barham, Jianmin Chen, Zhifeng Chen, Andy Davis, Jeffrey Dean, Matthieu Devin, Sanjay Ghemawat, Geoffrey Irving, Michael Isard, Manjunath Kudlur, Josh Levenberg, Rajat Monga, Sherry Moore, Derek G. Murray, Benoit Steiner, Paul Tucker, Vijay Vasudevan, Pete Warden, Martin Wicke, Yu Yuan, Xiaoqiang Zheng, TensorFlow: a system for large-scale machine learning, in: Proceedings of the 12th USENIX Conference on Operating Systems Design and Implementation (OSDI'16), USENIX Association, USA, 2016, pp. 265–283.
[25] P. Risholm, J. Balter, W.M. Wells, Estimation of delivered dose in radiotherapy: the influence of registration uncertainty, Med Image Comput Comput Assist Interv. 14 (Pt 1) (2011) 548–555, https://doi.org/10.1007/978-3-642-23623-5_69. PMID: 22003661; PMCID: PMC3265332.
[26] R. Krishnamurthy, N. Mummudi, J.S. Goda, S. Chopra, B. Heijmen, J. Swamidas, Using artificial intelligence for optimization of the processes and resource utilization in radiotherapy, JCO Glob Oncol 8 (2022 Nov) e2100393, https://doi.org/10.1200/GO.21.00393. PMID: 36395438; PMCID: PMC10166445.
[27] G. Bohara, A. Sadeghnejad Barkousaraie, S. Jiang, D. Nguyen, Using deep learning to predict beam-tunable Pareto optimal dose distribution for intensity-modulated radiation therapy, Med. Phys. 47 (9) (2020 Sep) 3898–3912, https://doi.org/10.1002/mp.14374. Epub 2020 Aug 2. PMID: 32621789; PMCID: PMC7821384.
[28] Y. Song, J. Hu, Y. Liu, H. Hu, Y. Huang, S. Bai, Z. Yi, Dose prediction using a deep neural network for accelerated planning of rectal cancer radiotherapy, Radiother. Oncol. 149 (2020 Aug) 111–116, https://doi.org/10.1016/j.radonc.2020.05.005. Epub 2020 May 19. PMID: 32416279.
[29] M.E. Ravari, S. Nasseri, M. Mohammadi, M. Behmadi, S.K. Ghiasi-Shirazi, M. Momennezhad, Deep-learning method for the prediction of three-dimensional dose distribution for left breast cancer conformal radiation therapy, Clin. Oncol. 35 (12) (2023 Dec) e666–e675, https://doi.org/10.1016/j.clon.2023.09.002. Epub 2023 Sep 15. PMID: 37741713.
[30] W. Yu, C. Xiao, J. Xu, J. Jin, X. Jin, L. Shen, Direct dose prediction with deep learning for postoperative cervical cancer underwent volumetric Modulated Arc Therapy, Technol. Cancer Res. Treat. 22 (2023 Jan-Dec) 15330338231167039, https://doi.org/10.1177/15330338231167039. PMID: 36999201; PMCID: PMC10071211.
[31] C. Jihong, B. Penggang, Z. Xiuchun, C. Kaiqiang, C. Wenjuan, D. Yitao, Q. Jiewei, Q. Kerun, Z. Jing, W. Tianming, Automated intensity modulated radiation therapy treatment planning for cervical cancer based on convolution neural network, Technol. Cancer Res. Treat. 19 (2020 Jan-Dec) 1533033820957002, https://doi.org/10.1177/1533033820957002. PMID: 33016230; PMCID: PMC7543127.
[32] Z. Qilin, B. Peng, Q. Ang, J. Weijuan, J. Ping, Z. Hongqing, D. Bin, Y. Ruijie, The feasibility study on the generalization of deep learning dose prediction model for volumetric modulated arc therapy of cervical cancer, J. Appl. Clin. Med. Phys. 23 (6) (2022 Jun) e13583, https://doi.org/10.1002/acm2.13583. Epub 2022 Mar 9. PMID: 35262273; PMCID: PMC9195039.
[33] H. Tang, Y. Chen, J. Jiang, K. Li, J. Zeng, Z. Hu, R. Yin, Dose prediction models based on geometric and plan optimization parameter for adjuvant radiotherapy planning design in cervical cancer radiotherapy, J Healthc Eng 2021 (2021 Nov 12) 7026098, https://doi.org/10.1155/2021/7026098. Retraction in: J Healthc Eng. 2023 May 24;2023:9865373. PMID: 34804459; PMCID: PMC8604605.
[34] A.M. Barragán-Montero, D. Nguyen, W. Lu, M.H. Lin, R. Norouzi-Kandalan, X. Geets, E. Sterpin, S. Jiang, Three-dimensional dose prediction for lung IMRT patients with deep neural networks: robust learning from heterogeneous beam configurations, Med. Phys. 46 (8) (2019 Aug) 3679–3691, https://doi.org/10.1002/mp.13597. Epub 2019 Jun 17. PMID: 31102554.
[35] J. Zhou, Z. Peng, Y. Song, Y. Chang, X. Pei, L. Sheng, X.G. Xu, A method of using deep learning to predict three-dimensional dose distributions for intensity-modulated radiotherapy of rectal cancer, J. Appl. Clin. Med. Phys. 21 (5) (2020 May) 26–37, https://doi.org/10.1002/acm2.12849. Epub 2020 Apr 13. PMID: 32281254; PMCID: PMC7286006.
[36] H. Yan, S. Liu, J. Zhang, J. Liu, T. Li, Utilizing pre-determined beam orientation information in dose prediction by 3D fully-connected network for intensity modulated radiotherapy, Quant Imaging Med Surg 11 (12) (2021 Dec) 4742–4752, https://doi.org/10.21037/qims-20-1076. PMID: 34888186; PMCID: PMC8611467.
[37] L. Redapi, L. Rossi, L. Marrazzo, J.J. Penninkhof, S. Pallotta, B. Heijmen, Comparison of volumetric modulated arc therapy and intensity-modulated radiotherapy for left-sided whole-breast irradiation using automated planning, Strahlenther. Onkol. 198 (3) (2022 Mar) 236–246, https://doi.org/10.1007/s00066-021-01817-x. Epub 2021 Aug 5. PMID: 34351452; PMCID: PMC8863712.